

Chapter 3

Classical Cyclotron

Abstract This chapter is an introduction to the classical cyclotron, with hints at spin dynamics, hands-on: by numerical simulation. It begins with a brief reminder of the historical context, and then introduces the theoretical material needed for the subsequent simulation exercises.

Basic charged particle optics and acceleration concepts are addressed in this chapter, including

- closed orbit in a cyclic accelerator,
- weak focusing in a dipole magnet,
- periodic transverse motion,
- revolution period and isochronism,
- voltage gap and resonant acceleration,
- the cyclotron equation.

The simulation of a cyclotron dipole just requires the optical element DIPOLE, which provides an analytical modeling of the field. TOSCA keyword could be preferred on the other hand, if a 2D or 3D, computed or measured field map of the magnet is available. The only other optical element which will be needed in the exercises in this chapter, is CAVITE, to simulate an oscillating voltage gap. The simulations generate a variety of output files, including the default output listing zgoubi.res, and optional output files such as zgoubi.plt produced by setting IL=2 in optical elements, zgoubi.CAVITE.out produced by CAVITE, zgoubi.MATRIX.out produced by MATRIX, and other similar zgoubi*.out files aimed at checking program execution, data post-treatment, producing graphs, etc. Additional keywords are introduced in the exercises, including FIT[2], a matching procedure; FAISCEAU which allows logging local particle coordinates in zgoubi.res; FAISTORE which logs local particle coordinates in a user defined file, usually for further external data treatment or plotting; MARKER; the 'system call' command SYSTEM; REBELOTE, a 'do loop'; and some more. Spin motion will be solved as well, this will require introducing SPNTRK, a request to do so while raytracing, and SPNPRT which prints out spin vector components to zgoubi.res.

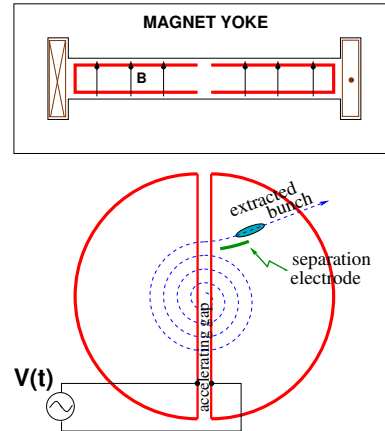
866 Notations used in the Text

$B; B_0$	field value; at reference radius R_0
$\mathbf{B}; B_R; B_y$	field vector; radial component; axial component
$B\rho = p/q$	particle rigidity
$C; C_0$	orbit length, $C = 2\pi R$; reference, $C_0 = 2\pi R_0$
E	particle energy
$f_{rf}; h$	RF frequency; RF harmonic number
$k = \frac{R}{B} \frac{dB}{dR}$	radial field index
$m; m_0; M$	mass; rest mass; in units of MeV/c^2
$\mathbf{p}; p; p_0$	particle momentum vector; its modulus; reference
q	particle charge
867 $R; R_0; R_E$	orbital radius; reference radius $R(p_0)$; at energy E
s	path variable
$\mathbf{v}; v$	particle velocity vector; its modulus
$V(t); \hat{V}$	oscillating voltage; its peak value
x, x', y, y'	radial and axial coordinates in the moving frame $[(*)' = d(*)/ds]$
$\beta = v/c; \beta_0; \beta_s$	normalized particle velocity; reference; synchronous
$\gamma = E/m_0$	Lorentz relativistic factor
$\Delta p, \delta p$	momentum offset
ε_u	Courant-Snyder invariant (u: x, r, y, l, Y, Z, s, etc.)
ϕ	RF phase at particle arrival at the voltage gap

868 Introduction

869 The cyclotron is the first cyclic accelerator. The concept: resonant acceleration of particles circling in a uniform magnetic field, goes back to the late 1920s [1]. The

Fig. 3.1 A sketch of the classical cyclotron. In the uniform magnetic field between two circular poles (top) an ion spirals out (bottom). A double-dee (or a single-dee facing a slotted electrode) forms a gap to which a fixed-frequency oscillating voltage $V(t)$ is applied. Its oscillation frequency is a harmonic of the revolution frequency. Particles experiencing proper voltage phase at the gap are accelerated. A septum electrode allows bunch extraction



870 first cyclotron was constructed at Berkeley, acceleration of H_2^+ hydrogen ions to
 871 80 keV [2] was achieved in 1931. The apparatus used a single dee vis-à-vis a slotted
 872 electrode forming a voltage gap, the ensemble housed in a 5 inch diameter vacuum
 873 chamber and placed in the 1.3 Tesla field of an electromagnet (Fig. 3.1). A ≈ 12 MHz
 874 vacuum tube oscillator a 1 kVolt peak gap voltage.

875 The goal foreseen in developing this technology was the acceleration of protons
 876 to MeV kinetic energy range for the study of atom nucleus - and in background a
 877 wealth of potential applications. An 11 inch cyclotron delivering a $0.01 \mu A$ H_2^+ beam
 878 at 1.22 MeV [3], and then a 27 inch cyclotron reaching 6 MeV (Fig. 3.2), followed [4].
 879 In the wake of Cockcroft and Walton first artificial disintegration experiment, targets
 880 were mounted at the periphery of the 11 inch cyclotron, disintegrations were observed
 881 in 1932. And in 1933: *'The neutron had been identified by Chadwick in 1932. By*
 882 *1933 we were producing and observing neutrons from every target bombarded by*
 883 *deuterons.*“ [4, M.S. Livingston,p. 22].

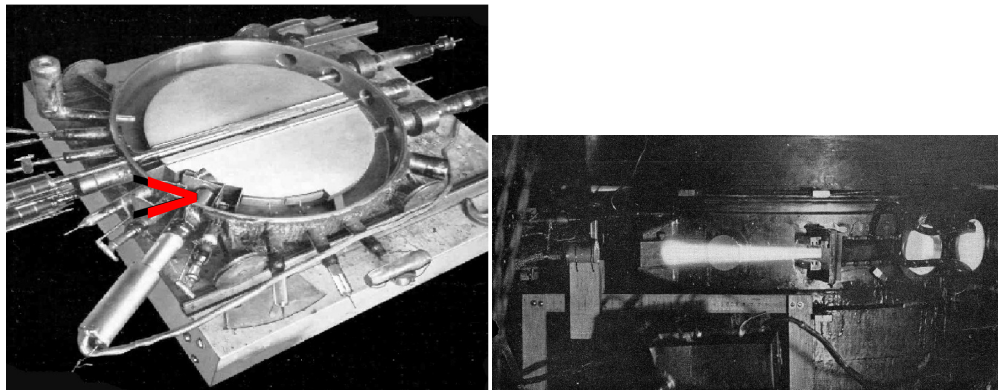


Fig. 3.2 Berkeley 27 inch cyclotron, first operated in 1934, accelerated deuterons up to 6 MeV. Left: a double-dee (seen in the vacuum chamber, cover off), 22 inch diameter, creates an accelerating gap: 13 kV, 12 MHz radio frequency voltage is applied for deuterons for instance (through two feed lines seen on the right). This apparatus was dipped in the 1.6 Tesla dipole field of a 27 in diameter (75 ton) electromagnet. A slight decrease of the dipole field with radius, from the center of the dees, assured vertical beam focusing. Particles spiral out from the center of the dees to the rim (where they strike a target, seen at the bottom on the left - arrow). Right: ionization of the air by the extracted beam (1936); the view also shows the vacuum chamber squeezed between the pole pieces of the electromagnet

884 The scope with accelerated beams from cyclotrons was broad: *“At this time*
 885 *biological experiments were started. I can recall the first time that a mouse was*
 886 *irradiated with neutrons. We put the mouse in a little cage and stuck him up on the*
 887 *side of the cyclotron tank and left him there for a while. Of course, nothing happened*
 888 *because [etc.]”* [4, McMillan,p.26]; and *“Also at about this same time the first*
 889 *radioactive tracer experiments on human beings were tried”* [op.cit.]; *“[...] simple*
 890 *beginnings of therapeutic use, coming a little bit later, in which neutron radiation was*
 891 *used, for instance, in the treatment of cancer. These things have gone on and built up*

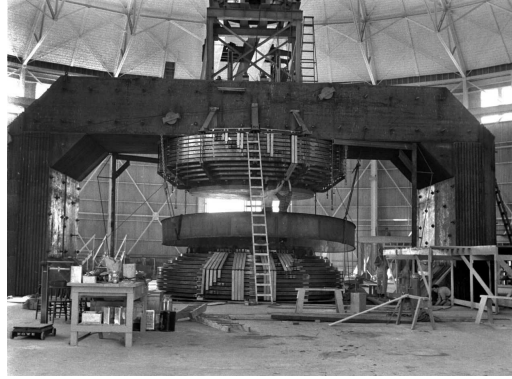


Fig. 3.3 Berkeley 184 in cyclotron. It was modified into a synchrocyclotron in 1946

so that there's now a whole field" [op.cit.]; and "Another highlight from 1936 was the first time that anyone tried to make artificially a naturally occurring radionuclide." (a bismuth isotope) [op.cit.]. The period also saw beam extraction developments (Fig. 3.2). Cyclotrons were constructed in many laboratories worldwide, from the early 1930s, following Berkeley demonstration.

Limitation in energy

An advanced theoretical understanding of the cyclotron more or less took until the mid-1930s, ending up with two news, a bad one and a good one, bad one first:

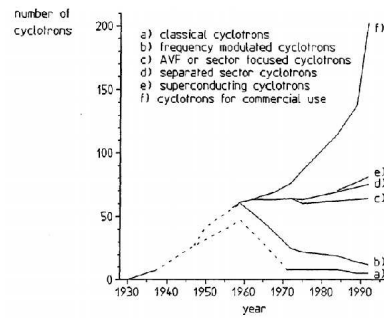
(i) the energy limitation, a consequence of the loss of isochronism resulting from the relativistic increase of the ion mass: "[...] it seems useless to build cyclotrons of larger proportions than the existing ones [...] an accelerating chamber of 37 in radius will suffice to produce deuterons of 11 MeV energy which is the highest possible [...]" [5] (related simulations will conclude this Chapter, "Classical Cyclotron"), or in a different form: "If you went to graduate school in the 1940s, this inequality ($-1 < k < 0$) was the end of the discussion of accelerator theory" [6].

The good news next:

(ii) the overcoming of that relativistic limit, due to L.H. Thomas in 1938 [7] - it took a few years though, to see practical effects.

Classical cyclotron technology has been in use for some time up to the few tens of MeV/u that it allows (Fig. 3.4), for such applications as neutron production for material science, radio-isotope production for medicine, injector stages in cyclotron complex facilities [9]. However with the progress in magnet computation tools and magnet fabrication (including permanent magnet techniques [10]), and the progress in computational speed and beam dynamics simulations (which includes accurate raytracing, as concerned in the present opus), the azimuthally varying field (AVF, or Thomas' [7]) cyclotron, much more performing, comes out to be essentially as simple and has in a general manner prevailed (Fig. 3.4).

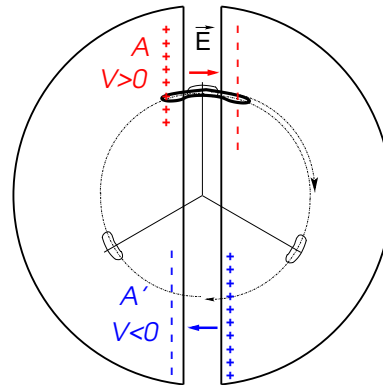
Fig. 3.4 Evolution of cyclotron species, over the years [8, Fig. 8]



3.1 Theory, Basic Concepts

The cyclotron was conceived as a means to overcome the inconvenient of using a long series of high voltage electrodes in a linear layout, by, instead, repeated recirculation using a magnetic field, for incremental, resonant, energy gain through a single accelerating gap. This gap is formed by a pair of cylindrical electrodes,

Fig. 3.5 Resonant acceleration: a positive ion bunch meets an accelerating field \vec{E} across gap A, at time t ; it meets again, half a revolution later, at time $t + T_{\text{rev}}/2$, an accelerating field across gap A', and so on so forth. In this $h = 1$ configuration, one bunch (and only one) over a turn is in synchronism with the accelerating phase of the oscillating voltage, at both gaps. Higher h allows more bunches: the next possibility with two dees would be $h=3$, and three stable bunches at 120 degrees from one another (thin contours) over a turn



“dees” (Fig. 3.5) which are applied a fixed frequency oscillating voltage, generated using a radio transmitter. The dees are placed in a uniform magnetic field which causes the ion bunches to follow, as they are accelerated, a piecewise-circular motion with increasing radius, normal to the field, more or less in phase with the voltage oscillation. An oscillating voltage is necessary as a DC voltage gap (a conservative field) in a circular accelerator can not yield energy gain: with the advent of resonant acceleration in the cyclotron and the development of cyclic accelerators in the horizon, it is interesting to note in passing that it is not possible to accelerate a particle

932 traveling on a closed path using an electrostatic field ($\mathbf{E} = -\mathbf{grad}V(\mathbf{R}, t)$ derives
 933 from a scalar potential), as the work by $\mathbf{F} = q\mathbf{E}$ only depends on the initial and final
 934 states, it does not dependent on the path followed (Fig. 3.6), which can be written

$$W = \int_P^Q \mathbf{F}.d\mathbf{s} = -q \int_P^Q \mathbf{grad}V.d\mathbf{s} = -q(V_Q - V_P) \quad (3.1)$$

935 On a closed path: $\oint \mathbf{F}.d\mathbf{s} = 0$, the force is conservative, no work is performed,
 936 consequence: a DC voltage gap in a circular machine does not yield energy gain.

937 Instead, the work of a force of induction origin, where $\mathbf{E} = -\partial\mathbf{A}/\partial t$ arises from
 938 the variation of a magnetic flux ($\mathbf{B} = \mathbf{curl} \mathbf{A}$, \mathbf{A} a vector potential), may be non-zero
 939 on a closed path. This is achieved for instance using a radio-frequency system which
 940 feeds an oscillating voltage across a gap, $V(t) = \hat{V} \sin(\omega_{rf}t + \phi)$ (Fig. 3.7).

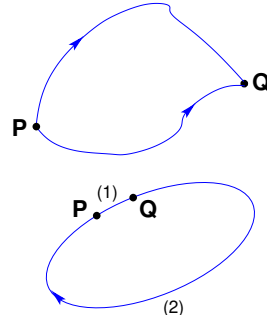


Fig. 3.6 Top: the work of the electrostatic force $\mathbf{F} = q\mathbf{E}$ is $W = \int_P^Q \mathbf{F}.d\mathbf{s} = -q(V_Q - V_P)$. Bottom: over closed path, the particle loses along (2) the energy gained along (1)

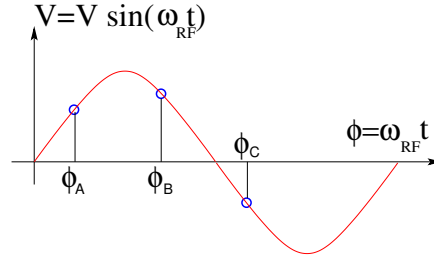


Fig. 3.7 A particle which reaches the double-dee gap at the RF phase $\omega_{rf}t = \phi_A$ or $\omega_{rf}t = \phi_B$ is accelerated. If it reaches the gap at $\omega_{rf}t = \phi_C$ it is decelerated

941 As an accelerated bunch spirals outward in a uniform magnetic field, the increase
 942 in the distance it travels over a turn is compensated by its velocity increase: in
 943 the non-relativistic approximation ($\beta \ll 1$), the revolution period T_{rev} increases
 944 only slowly with energy; with appropriate voltage frequency $f_{rf} \approx h/T_{rev}$ revolution
 945 motion and RF can be maintained in sufficiently close synchronism, $T_{rev} \approx hT_{rf}$, that
 946 the bunch will transit the accelerating gaps (Fig. 3.5) during the accelerating phase
 947 of the oscillating $V(t)$ (Fig. 3.7).

948 The orbital motion quantities: radius R , field B , particle rigidity BR , revolution
949 frequency $f_{\text{rev}} = \omega_{\text{rev}}/2\pi$, satisfy

$$BR = \frac{p}{q}, \quad 2\pi f_{\text{rev}} = \frac{v}{R} = \frac{qB}{m} = \frac{qB}{\gamma m_0} \quad (3.2)$$

These relationships hold at all γ , from $v \ll c$ ($\gamma \approx 1$, domain of the *classical* cyclotron) to $\gamma > 1$ (domain of the *isochronous* cyclotron). To give an idea of the revolution frequency, in the limit $\gamma = 1$ one has

$$\frac{f_{\text{rev}}}{B} = \frac{q}{2\pi m} = 15.25 \text{ MHz/T} \quad \text{for protons.}$$

950 The RF frequency $f_{\text{rf}} = \omega_{\text{rf}}/2\pi$ is constant in a cyclotron, whereas the revolution
951 period slowly increases with energy (Sec. 3.1.3). In the classical cyclotron f_{rf} is set,
952 by design, equal to hf_{rev} for an intermediate energy taken along the acceleration
953 cycle. The energy gain, or loss, by the particle when transiting the gap is

$$\Delta W = q\hat{V} \sin \phi(t) \quad \text{with } \phi(t) = \omega_{\text{rf}}t - \omega_{\text{rev}}t + \phi_0 \quad (3.3)$$

954 with ϕ its phase with respect to the RF signal at the gap (e.g., ϕ_A , ϕ_B or ϕ_C in
955 Fig. 3.7) and ϕ_0 the value at $t = 0$, $\omega_{\text{rev}}t$ the orbital angle advance.

Fixed-frequency acceleration requires the RF and cyclotron frequencies to be matched to one another. However the relativistic increase of the mass upon velocity increase causes the revolution period to increase with momentum: in $T_{\text{rev}} = 2\pi m/qB$, B is almost constant and m increases, resulting in a turn-by-turn

$$\frac{\Delta T_{\text{rev}}}{T_{\text{rev}}} = \gamma - 1$$

956 The mis-match between the accelerating RF and cyclotron frequencies is a
957 turn-by-turn cumulative effect and sets a limit to the tolerable isochronism defect,
958 $\Delta T_{\text{rev}}/T_{\text{rev}} \approx 2 - 3\%$, or highest velocity $\beta = v/c \approx 0.22$. This results for instance in
959 a practical limitation of the “classical cyclotron” to an upper ≈ 25 MeV for protons,
960 and ≈ 50 MeV for D and α particles.

961 To conclude on these basis concepts regarding acceleration, multiple accelerating
962 gap structures is part of the evolutions of the classical cyclotron, where a “D” is
963 rather a “ Δ ” pattern, and towards high RF frequency harmonic. An example among
964 many others is, as an illustration, GANIL C0 injector with its 4 accelerating gaps
965 and h=4 and h=8 RF operation [9].

966 3.1.1 Fixed-Energy Orbits, Revolution Period

967 The differential equations of particle motion are established in the Serret-Frénet
968 frame, Sec. 3.1.2, however, some basic geometrical properties can be derived in the

laboratory frame, as follows. In the laboratory frame (O;x,y,z), with (O;x,z) the bend plane, assume $\mathbf{B}|_{y=0} = \mathbf{B}_y$. A particle is launched from the origin with a velocity $\mathbf{v} = (v \sin \alpha, 0, v \cos \alpha)$ at an angle α from the longitudinal axis z (Fig. 3.8).

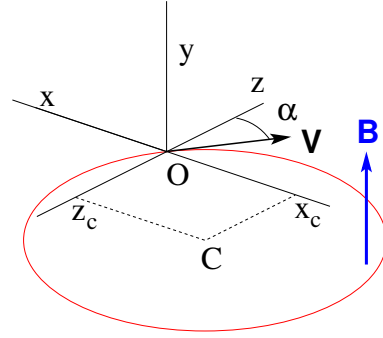


Fig. 3.8 Circular motion of a charged particle in the plane normal to a uniform magnetic field \mathbf{B} . The circle center is at $x_C = -v \cos \alpha / \omega_{\text{rev}}$, $z_C = v \sin \alpha / \omega_{\text{rev}}$.

Solving

$$m\dot{\mathbf{v}} = q\mathbf{v} \times \mathbf{B} \quad (3.4)$$

with $\mathbf{v} = (\dot{x}, \dot{y}, \dot{z})$, $\mathbf{B} = (0, B_y, 0)$ yields the parametric equations of motion

$$\begin{cases} x(t) = \frac{v}{\omega_{\text{rev}}} \cos(\omega_{\text{rev}}t - \alpha) - \frac{v \cos \alpha}{\omega_{\text{rev}}} \\ z(t) = \frac{v}{\omega_{\text{rev}}} \sin(\omega_{\text{rev}}t - \alpha) + \frac{v \sin \alpha}{\omega_{\text{rev}}} \\ y(t) = \text{constant} \end{cases} \quad (3.5)$$

which results in

$$\left(x + \frac{v \cos \alpha}{\omega_{\text{rev}}}\right)^2 + \left(z - \frac{v \sin \alpha}{\omega_{\text{rev}}}\right)^2 = \left(\frac{v}{\omega_{\text{rev}}}\right)^2 \quad (3.6)$$

a circular trajectory of radius $R = p/qB$ centered at $x = -v \cos \alpha / \omega_{\text{rev}}$, $z = v \sin \alpha / \omega_{\text{rev}}$, revolution period

$$T_{\text{rev}} = \frac{2\pi}{\omega_{\text{rev}}} = \frac{2\pi m}{qB}$$

Cyclic motion - Horizontal motion in uniform field has no privileged reference orbit: for a given momentum, the initial radius and velocity vector define a particular closed, circular orbit. A particle launched with an axial velocity component v_y on the other hand, drifts vertically linearly with time, as there is no axial restoring force. The next

979 Section will investigate the necessary field property, absent in our simplified field
 980 model so far, proper to ensure confinement of the multiturn 6-dimensional periodic
 981 motion in the vicinity of the median plane of the cyclotron dipole magnet.

982 3.1.2 Weak Focusing, Transverse Motion

983 In the lower energy (smaller radius) accelerated turns in a classical cyclotron, the
 984 electric field in the accelerating gap contributes proper transverse focusing so that
 985 the magnet gap can be designed parallel (an example can be found in Ref. [9]). In
 986 very low energy applications even, extraction energy in the tens of keV/u range where
 987 electric fields are still effective, flat magnetic field with uniformity $dB/B < 10^{-4}$
 988 can be achieved over the (reduced) extent of the cyclotron orbit and maintains proper
 989 isochronism. Beyond this low energy region however, at greater radius, a magnetic
 990 field gradient must be introduced, field decreasing with R, by shaping the magnet
 991 poles, to ensure proper vertical focusing. Note that because of the field decreases
 992 with R in a parallel gap, as discovered *a posteriori*, the very first cyclotrons were
 993 working [11]. This section introduces to these magnetic focusing principles.

994 In the following, $B_R(R)$, $B_y(R)$ denote the radial and axial components of the
 995 magnetic field at radius R. Median-plane symmetry of the field is assumed, thus
 996 $B_R|_{y=0} = 0$ at all R (Fig. 3.9). Particle coordinates are defined in the Serret-Frénet
 997 frame (O;s,x,y), moving along the R_0 radius reference orbit (the origin O is at the
 998 location of the reference particle, s axis tangent to the reference orbit, x axis radial,
 999 y axis normal to the bend plane, Fig. 3.10). The radial excursion of a particle with
 1000 respect to the reference orbit writes

$$x(t) = R(t) - R_0 \ll R_0 \quad (3.7)$$

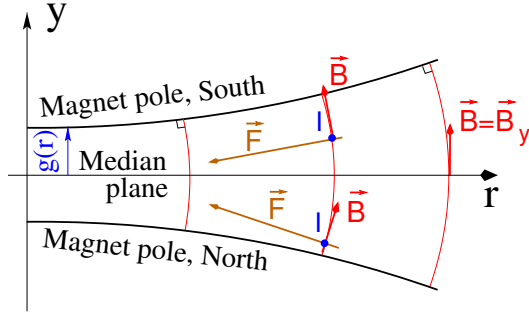
1001 Considering small radial and axial excursions from ($R = R_0, y = 0$), a Taylor
 1002 expansion of the magnetic field can be introduced,

$$\begin{aligned} B_y(R_0 + x) &= B_y(R_0) + x \left. \frac{\partial B_y}{\partial R} \right|_{R_0} + \frac{x^2}{2!} \left. \frac{\partial^2 B_y}{\partial R^2} \right|_{R_0} + \dots \approx B_y(R_0) + x \left. \frac{\partial B_y}{\partial R} \right|_{R_0} \\ B_R(0 + y) &= y \underbrace{\left. \frac{\partial B_R}{\partial y} \right|_0}_{= \left. \frac{\partial B_y}{\partial R} \right|_{R_0}} + \frac{y^3}{3!} \left. \frac{\partial^3 B_R}{\partial y^3} \right|_0 + \dots \approx y \left. \frac{\partial B_y}{\partial R} \right|_{R_0} \end{aligned} \quad (3.8)$$

1003 Using this approximation, the differential equations of motion in the moving frame
 1004 can be written under the form, linear in x and y ,

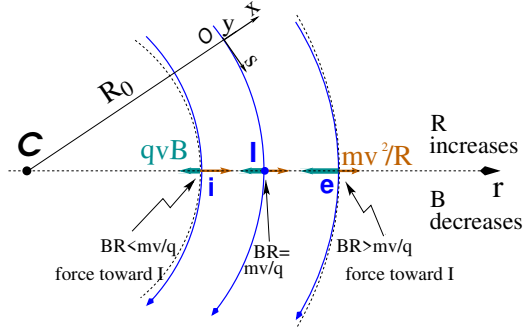
$$\begin{aligned}
F_x = m\ddot{x} &= -qvB_y(R) + \frac{mv^2}{R_0 + x} \approx -qv \left(B_y(R_0) + \left. \frac{\partial B_y}{\partial R} \right|_{R_0} x \right) + \frac{mv^2}{R_0} \left(1 - \frac{x}{R_0} \right) \\
\rightarrow m\ddot{x} &= -\frac{mv^2}{R_0^2} \left(\frac{R_0}{B_0} \left. \frac{\partial B_y}{\partial R} \right|_{R_0} + 1 \right) x \quad (3.9) \\
F_y = m\ddot{y} &= qvB_R(y) = qv \left. \frac{\partial B_R}{\partial y} \right|_{y=0} y + \text{higher order} \rightarrow m\ddot{y} = qv \frac{\partial B_y}{\partial R} y
\end{aligned}$$

Fig. 3.9 Axial motion stability requires proper shaping of field lines: B has to decrease with radius. The Laplace force pulls a charge at I (velocity pointing out of the page) toward the median plane. Increasing the field gradient (i.e. closer to -1, gap opening up faster) increases the focusing



1005

Fig. 3.10 Radial motion stability in an axially symmetric structure. Arrowed arcs are trajectories of particles with momentum $p=mv$. Dashed arcs are centered at C , center of the cyclotron. The resultant $F_t = -qvB + mv^2/r$, is zero at I : $B_0 R_0 = mv/q$. The resultant at i is toward I if $qvB_i < mv^2/R_i$, i.e. $B_i R_i < mv/q$; the resultant at e is toward I if $qvB_e > mv^2/R_e$, i.e. $B_e R_e > mv/q$



1006

Note $B_y(R_0) = B_0$ and introduce

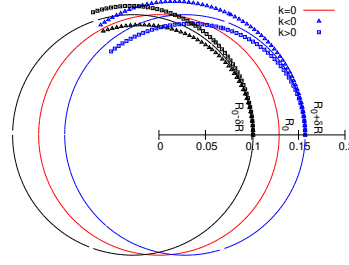
$$\omega_R^2 = \omega_{\text{rev}}^2 \left(1 + \frac{R_0}{B_0} \frac{\partial B_y}{\partial R} \right), \quad \omega_y^2 = -\omega_{\text{rev}}^2 \frac{R_0}{B_0} \frac{\partial B_y}{\partial R} \quad (3.10)$$

1007

equations 3.9 can thus be written under the form

$$\ddot{x} + \omega_R^2 x = 0 \quad \text{and} \quad \ddot{y} + \omega_y^2 y = 0 \quad (3.11)$$

Fig. 3.11 Geometrical focusing: in a flat field, $k=0$, the two circular trajectories at $r = R_0 \pm \delta R$ (solid lines) undergo exactly one oscillation around the reference orbit $r = R_0$. A positive k increases the convergence (square markers - but then the vertical motion diverges from the median plane), a negative k decreases the convergence (triangles)



1008 A restoring force (linear terms in x and y , Eq. 3.11) arises from the radially varying
1009 field, characterized by a field index

$$k = \frac{R_0}{B_0} \frac{\partial B_y}{\partial R} \Big|_{R=R_0, y=0} \quad (3.12)$$

1010 and adds in the radial motion to the focusing due to the curvature (the term “1” in
1011 ω_R^2 , Eq. 3.10).

1012 *Axial stability* in a cyclotron requires a restoring force directed toward the median
1013 plane. Referring to Fig. 3.9, this means $F_y = -ay$ (with the a factor some positive
1014 quantity) and thus $B_R < 0$, at all $(r, y \neq 0)$. This is achieved by designing a guiding
1015 field which decreases with radius, $\frac{\partial B_R}{\partial y} < 0$. Referring to Eq. 3.12 this translates into
1016 $k < 0$.

1017 *Radial stability* in a constant field is a geometrical property, resulting from the
1018 curvature of the trajectory (Fig. 3.11). In a weakly decreasing field $B(R)$ on the
1019 other hand, a particle with momentum $p = mv$ sinusoiding around the R_0 -radius
1020 reference circle experiences in the Serret-Frénet frame a total force $F_t = -qvB + m \frac{v^2}{r}$
1021 (Fig. 3.10) of which the (outward) component $f_c = m \frac{v^2}{r}$ decreases with r at a higher
1022 rate than the decrease of the Laplace (inward) component $f_B = -qvB(r)$. In other
1023 words, radial stability requires BR to increase with R , $\frac{\partial BR}{\partial R} = B + R \frac{\partial B}{\partial R} \geq 0$, this
1024 holds in particular at R_0 , thus $1 + k \geq 0$.

1025 The condition for transverse motion stability around the circular equilibrium orbit
1026 results from these axial and radial stability conditions, namely,

$$-1 \leq k < 0 \quad (3.13)$$

Note regarding the geometrical focusing: the focal distance associated with the curvature of a magnet of arc length \mathcal{L} is obtained by integrating $\frac{d^2 x}{ds^2} + \frac{1}{R_0^2} x = 0$ and identifying with the focusing property $\Delta x' = -x/f$, namely,

$$\Delta x' = \int \frac{d^2 x}{ds^2} ds \approx \frac{-x}{R^2} \int ds = \frac{-x \mathcal{L}}{R^2}, \text{ thus } f = \frac{R^2}{\mathcal{L}}$$

1027 *Isochronism*

1028 The relativistic increase of the mass precludes strict isochronism: the revolution
 1029 frequency slowly decreases with the energy of the particle on its spiraling out
 1030 trajectory (Eq. 3.2). The focusing condition $-1 < k < 0$ (B decreasing with R) further
 1031 contributes breaking the isochronism by virtue of $\omega_{\text{rev}} \propto B$. As a consequence, the
 1032 phase of the oscillating voltage at arrival of a particle at the accelerating gap (the
 1033 so-called RF phase) changes turn after turn. This is addressed further in Sec. 3.1.3.

1034 **Paraxial Transverse Coordinates**

1035 Introducing the path variable, s , as the independent variable in Eq. 3.11 and using
 1036 the approximation $ds \approx v dt$ (*i.e.*, neglecting the transverse velocity components), the
 1037 equations of motion in the moving frame (Eq. 3.11) take the form

$$\frac{d^2 x}{ds^2} + \frac{1+k}{R_0^2} x = 0 \quad \text{and} \quad \frac{d^2 y}{ds^2} - \frac{k}{R_0^2} y = 0 \quad (3.14)$$

1038 Given $-1 < k < 0$ the motion is that of a harmonic oscillator, in both planes, with
 1039 respective restoring constants $(1+k)/R_0^2$ and $-k/R_0^2$, both positive quantities. The
 1040 solution is a sinusoidal motion,

$$\begin{cases} R(s) - R_0 = x(s) = x_0 \cos \frac{\sqrt{1+k}}{R_0} (s - s_0) + x'_0 \frac{R_0}{\sqrt{1+k}} \sin \frac{\sqrt{1+k}}{R_0} (s - s_0) \\ R'(s) = x'(s) = -x_0 \frac{\sqrt{1+k}}{R_0} \sin \frac{\sqrt{1+k}}{R_0} (s - s_0) + x'_0 \cos \frac{\sqrt{1+k}}{R_0} (s - s_0) \end{cases} \quad (3.15)$$

$$\begin{cases} y(s) = y_0 \cos \frac{\sqrt{-k}}{R_0} (s - s_0) + y'_0 \frac{R_0}{\sqrt{-k}} \sin \frac{\sqrt{-k}}{R_0} (s - s_0) \\ y'(s) = -y_0 \frac{\sqrt{-k}}{R_0} \sin \frac{\sqrt{-k}}{R_0} (s - s_0) + y'_0 \cos \frac{\sqrt{-k}}{R_0} (s - s_0) \end{cases} \quad (3.16)$$

1042 The dissymmetry between the two frequencies, a “1” in “ $\sqrt{1+k}$ ” compared to $\sqrt{-k}$,
 1043 stems from the geometrical focusing resulting from the curvature.

1044 Two wave numbers may be introduced,

$$\nu_R = \frac{\omega_R}{\omega_{\text{rev}}} = \sqrt{1+k} \quad \text{and} \quad \nu_y = \frac{\omega_y}{\omega_{\text{rev}}} = \sqrt{-k} \quad (3.17)$$

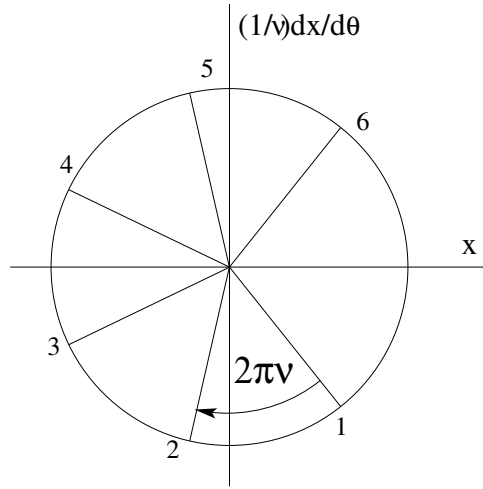
1045 *i.e.*, the number of sinusoidal oscillations of the paraxial motion about the reference
 1046 circular orbit over a turn, respectively radial and axial. Both are less than 1: there
 1047 is less than one sinusoidal oscillation in a revolution. In addition, as a result of the
 1048 revolution symmetry,

$$\nu_R^2 + \nu_y^2 = 1 \quad (3.18)$$

1049 Phase Space

1050 Phase space at an azimuth s around the ring is a Cartesian space with, regarding
 1051 transverse particle motion, position as the horizontal axis and angle as the vertical
 1052 axis, *i.e.*, $(x(s), x'(s) = dx/ds)$ and $(y(s), y'(s) = dy/ds)$ (Eqs. 3.15 3.16), or akin
 1053 quantities, this is illustrated in Fig. 3.12.

Fig. 3.12 Particle motion observed in transverse horizontal phase space at some fixed azimuth $s = R\theta_{\text{obs}}$ along the cyclotron circumference, at successive times (or turns: 1, 2, 3, ...). The horizontal axis here is $x(\theta_{\text{obs}})$, the vertical axis is $\frac{1}{\nu_R} \frac{dx}{d\theta} \Big|_{\theta=\theta_{\text{obs}}}$, using these coordinates the motion is on a circle of radius \hat{x} . Note that $\{x(\theta_{\text{obs}}) = \hat{x} \cos(\nu_R \theta_{\text{obs}} + \phi)$ and $\frac{1}{\nu_R} \frac{dx}{d\theta} \Big|_{\theta=\theta_{\text{obs}}} = -\hat{x} \sin(\nu_R \theta_{\text{obs}} + \phi)\}$ establishes that phase space motion is clockwise



1054 Longitudinal phase space coordinates are the RF phase ϕ (Fig. 3.7, Eq. 3.3) and
 1055 energy offset, or akin quantities.

1056 A point in phase space represents the position of a particle at azimuth s at time t .

1057 Particle motion over time depends on the field experienced and on two initial
 1058 conditions (initial position and angle, or RF phase and energy offset, ...). It is
 1059 impossible for two trajectories with different origins to coincide in phase space, at
 1060 any azimuth.

1061 Off-Momentum Motion

1062 Momenta of particles that make up a bunch accelerated in a cyclotron span some
 1063 extent $\pm \Delta p/p$.

In an axially symmetric structure, the equilibrium trajectory at momentum

$$\begin{cases} p_A \\ p_B = p_A + \Delta p \end{cases} \text{ is at radius } \begin{cases} R_A \text{ such that } B_A R_A = p_A/q \\ R_B \text{ such that } B_B R_B = p_B/q \end{cases}, \text{ with } \begin{cases} B_B = B_A + \left(\frac{\partial B}{\partial x} \right)_0 + \dots \\ R_B = R_A + \Delta x \end{cases}$$

On the other hand

$$B_B R_B = \frac{p_B}{q} \Rightarrow \left[B_A + \left(\frac{\partial B}{\partial x} \right)_0 \Delta x + \dots \right] (R_A + \Delta x) = \frac{p_A + \Delta p}{q} = \frac{p_A}{q} + \frac{\Delta p}{q}$$

thus, neglecting terms in $(\Delta x)^2$,

$$B_A R_A + \left(\frac{\partial B}{\partial x} \right)_0 R_A \Delta x + B_A \Delta x = \frac{p_A}{q} + \frac{\Delta p}{q},$$

1064 which, given $B_A R_A = \frac{p_A}{q}$, leaves $\Delta x \left[\left(\frac{\partial B}{\partial x} \right)_0 R_A + B_A \right] = \frac{\Delta p}{q}$, which given $k =$
 1065 $\frac{R_A}{B_A} \left(\frac{\partial B}{\partial x} \right)_0$ yields

$$\Delta x = \frac{R_A}{1 + k} \frac{\Delta p}{p_A} \quad (3.19)$$

Drop the indices, take p as a reference momentum and R as the corresponding

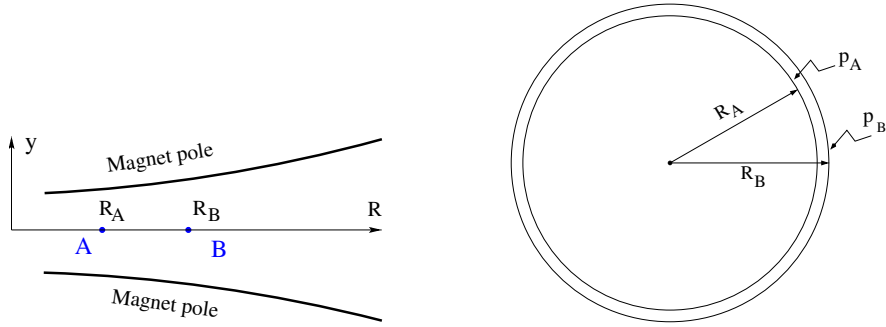


Fig. 3.13 The equilibrium radius at location A is $R = R_A$, the equilibrium momentum is p_A , rigidity $BR = B_A R_A$. The equilibrium radius at B is $R = R_B$, equilibrium momentum p_B , rigidity $BR = B_B R_B$

1066 reference orbit radius, this leaves
 1067

$$\Delta x = D \frac{\Delta p}{p} \quad \text{with} \quad D = \frac{R}{1 + k}, \quad \text{dispersion function} \quad (3.20)$$

1068 The dispersion D is an s -independent quantity in the classical cyclotron as a result of
 1069 the cylindrical symmetry of the field (k and $R=p/qB$ are s -independent), and varies
 1070 with R and $k(R)$.

1071 To the first order in the coordinates, the vertical coordinates $y(s)$, $y'(s)$ (Eq. 3.16)
 1072 are unchanged under the effect of a momentum offset, the horizontal trajectory angle
 1073 $x'(s)$ is unchanged as well (the circular orbits are concentric, Fig. 3.13) whereas

$$x(s, p + \Delta p) = x(s, p) + \Delta p \left. \frac{dx}{dp} \right|_{s,p} = x(s) + D \frac{\Delta p}{p} \quad (3.21)$$

1074 with $x(s)$ as in Eq. 3.15.

1075 *Orbit and revolution period lengthening*

1076 Momentum offset results in closed orbit lengthening $\delta C/C = \delta R/R \equiv \delta x/R$, which,
1077 given Eq. 3.20, can be written under the form

$$\frac{\delta C}{C} = \alpha \frac{\delta p}{p} \quad \text{with} \quad \alpha = \frac{1}{1+k} = \frac{1}{v_R^2} \quad (3.22)$$

1078 with α the “momentum compaction” and $\alpha > 0$, the closed orbit length increases
1079 with momentum.

1080 The change in revolution period $T_{\text{rev}} = C/\beta c$ with momentum writes

$$\frac{\delta T_{\text{rev}}}{T_{\text{rev}}} = \frac{\delta C}{C} - \frac{\delta \beta}{\beta} = \left(\alpha - \frac{1}{\gamma^2}\right) \frac{\delta p}{p} \quad (3.23)$$

1081 Given that $-1 < k < 0$ and $\gamma \gtrsim 1$, it results that $\alpha - 1/\gamma^2 > 0$ thus $\delta T_{\text{rev}}/T_{\text{rev}} > 0$ as
1082 expected: the revolution period increases with energy, the increase in radius is faster
1083 than the velocity increase.

1084 3.1.3 Quasi-Isochronous Resonant Acceleration

1085 An oscillating radio-frequency (RF) electric field, with fixed-frequency f_{rf} is applied
1086 across the gap between the two dees (Fig. 3.1). An ion of charge q reaching the gap
1087 at time t undergoes a change in energy

$$\Delta W(t) = q\hat{V} \sin \phi, \quad \text{with} \quad \phi = \omega_{\text{rf}}t - (\omega_{\text{rev}}t + \phi_0) \quad (3.24)$$

1088 with ϕ the RF phase experienced by the particle at the time it crosses the gap and ϕ_0
1089 the origin in phase for the particle motion. This ignores the “transit time”, the effect
1090 of the time that the particle spends across the gap on the overall energy gain.

1091 The frequency dependence of the kinetic energy W of the ion relates to its orbital
1092 radius R in the following way:

$$W = \frac{1}{2}mv^2 = \frac{1}{2}m(2\pi R f_{\text{rev}})^2 = \frac{1}{2}m(2\pi R \frac{f_{\text{rf}}}{h})^2 \quad (3.25)$$

1093 thus, given cyclotron size (R), f_{rf} and h set the limit for the acceleration range.

1094 The revolution frequency decreases with energy and the condition of synchronism
1095 with the oscillating voltage, $f_{\text{rf}} = hf_{\text{rev}}$, is only fulfilled at one particular radius in the
1096 course of acceleration, where $\omega_{\text{rf}} = qB/m$ (Fig. 3.14). Upstream and downstream
1097 of that radius, out-phasing $\Delta\phi$ builds-up turn after turn, decreasing in a first stage

(towards lower voltages in Fig. 3.14-right) and then increasing back to $\phi = \pi/2$ and beyond towards π . Beyond $\phi = \pi$ the RF voltage is decelerating.

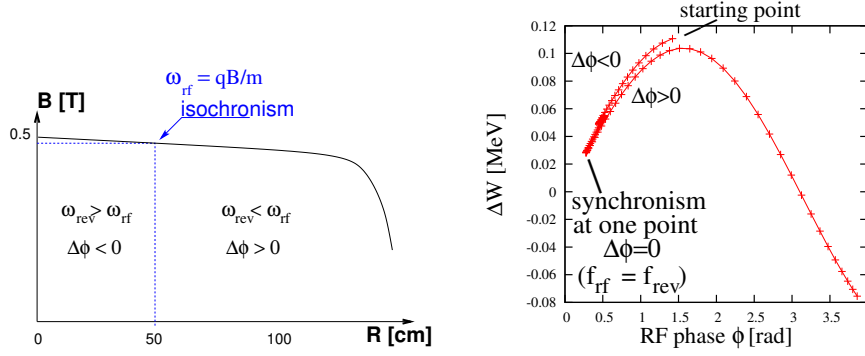


Fig. 3.14 A sketch of the synchronism condition at one point (left, $h=1$ assumed), and the span in phase of the energy gain $\Delta W = q\hat{V} \sin \phi$ over the acceleration cycle (right). ϕ is the phase of the RF sine wave at arrival of the particle at the accelerating gap (the vertical separation of the two $\Delta W(\phi)$ branches on the right ($\Delta\phi < 0$ and $\Delta\phi > 0$) is artificial, this is for clarity, they are actually superimposed)

Differentiating the particle phase at the RF gap (Eq. 3.24), over a half-turn, with ω_{rev} constant between two gap passages, one gets $\dot{\phi} = \omega_{rf} - \omega_{rev}$. Between two gap passages on the other hand, $\Delta\phi = \dot{\phi}\Delta T = \dot{\phi}T_{rev}/2 = \dot{\phi}\frac{\pi R}{v}$, yielding a phase-shift of

$$\text{half-turn } \Delta\phi = \pi \left(\frac{\omega_{rf}}{\omega_{rev}(R)} - 1 \right) = \pi \left(\frac{m\omega_{rf}}{qB(R)} - 1 \right) \quad (3.26)$$

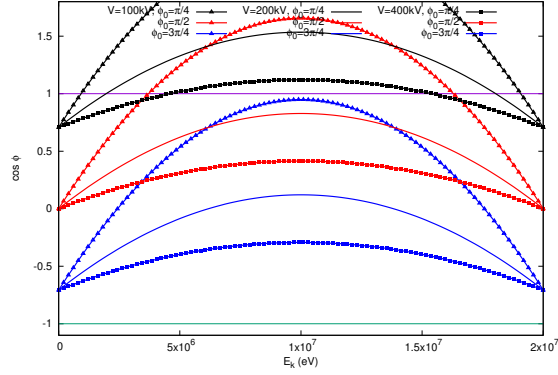
The out-phasing is thus a gap-after-gap, cumulative effect. Due to this the classical cyclotron requires quick acceleration (limited number of turns), which means high voltage (tens to hundreds of kVolts). As expected, with ω_{rf} and B constant, ϕ presents a minimum ($\dot{\phi} = 0$) at $\omega_{rf} = \omega_{rev} = \frac{qB}{m}$ where exact isochronism is reached (Fig. 3.14). The upper limit to ϕ is set by the condition $\Delta W > 0$: acceleration.

The cyclotron equation determines the achievable energy range, depending on the injection energy E_0 , the RF phase at injection ϕ_0 , the RF frequency ω_{rf} and gap voltage \hat{V} , following [12]

$$\cos \phi = \cos \phi_0 + \pi \left[1 - \frac{\omega_{rf}}{\omega_{rev}} \frac{E + E_0}{2M} \right] \frac{E - E_0}{q\hat{V}} \quad (3.27)$$

($E=E_k + M$ is the total energy, M is the rest mass, the index 0 denotes injection parameters) and is represented in Fig. 3.15 for various values of the RF voltage and phase at injection ϕ_0 .

Fig. 3.15 A graph of the cyclotron equation (Eq. 3.27), for a few different RF settings. The sole settings resulting in a $\cos \phi$ curve comprised in $[-1, 1]$ allow complete acceleration from injection to top energy. For instance, for injection $\phi_0 = \pi/4$, acceleration to 20 MeV is not possible (upper three curves). Acceleration to 20 MeV works with $\phi_0 = 3\pi/4$, with as low as 100 kV/gap (lower three curves)



3.1.4 Extraction

From $R = p/qB$ and assuming constant field (this is legitimate in the presence of a very small field index), with kinetic energy $E_k = p^2/2M$ in the non-relativistic approximation ($E_k \ll M$), one gets

$$\frac{dR}{R} = \frac{1}{2} \frac{dE_k}{E_k} \quad (3.28)$$

Integrating the right hand side equality yields

$$R^2 = R_0^2 \frac{E_k}{E_{k,0}} \quad (3.29)$$

with $R_0, E_{k,0}$ initial conditions. From Eqs. 3.28, 3.29, assuming $E_{k,0} \ll E_k$ and constant acceleration rate dE_k such that $E_k = n dE_k$ after n turns, one gets the scaling laws

$$R \propto \sqrt{n}, \quad dR \propto \frac{R}{E_k} \propto \frac{1}{R} \propto dE_k, \quad \frac{dR}{dn} = \frac{R}{2n} \quad (3.30)$$

so that, in particular, the turn separation dR/dn is proportional to the average orbit radius R and to the energy gain per turn.

The radial distance between successive turns decreases with energy, toward zero (Fig. 3.16), eventually resulting in insufficient spacing for insertion of an extraction septum.

Betatron modulation

Consider a particle bunch injected in the cyclotron with some (x_0, x'_0) conditions, and assume very slow acceleration. While accelerated the bunch undergoes a betatron

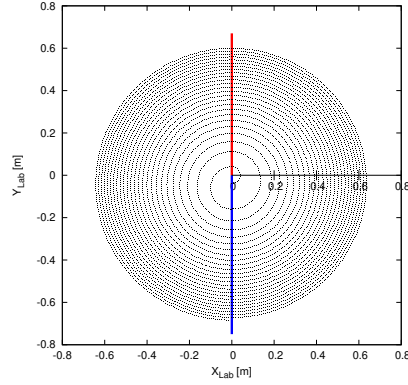


Fig. 3.16 The radial distance between successive turns decreases with energy, in inverse proportion to the orbit radius

1130 motion around the local closed orbit, following Eq. 3.15. Observed at some azimuth
 1131 s , this betatron oscillation modulates the distance of the bunch to the local reference
 1132 closed orbit, moving it outward or inward depending on the turn number, which
 1133 means a modulation of the distance between the accelerated turns: an effect that
 1134 can be exploited for increasing the separation of consecutive orbits at extraction to
 1135 enhance the extraction efficiency [8].

1136 3.1.5 Spin Dance

1137 An effect of a magnetic field \mathbf{B} on a spin angular momentum \mathbf{S} , as a consequence of
 1138 the resulting torque, is the spin precession, around the precession vector (Sec. 20.6.1)

$$\omega_{\text{sp}} = \frac{q}{m} [\mathbf{B} + G(\mathbf{B}_{\parallel} + \gamma\mathbf{B}_{\perp})] \quad (3.31)$$

1139 at an angular frequency $|\omega_{\text{sp}}|$, with $\mathbf{B} = \mathbf{B}_{\parallel} + \mathbf{B}_{\perp}$, \mathbf{B}_{\parallel} and \mathbf{B}_{\perp} the magnetic field
 1140 components respectively parallel and normal to the particle velocity, and G the
 1141 anomalous gyromagnetic factor:

1142 $G=1.7928474$ (proton), -0.178 (Li), -0.143 (deuteron), -4.184 (^3He) ...

1143 The spin precession in \mathbf{B} satisfies the Thomas-BMT differential equation

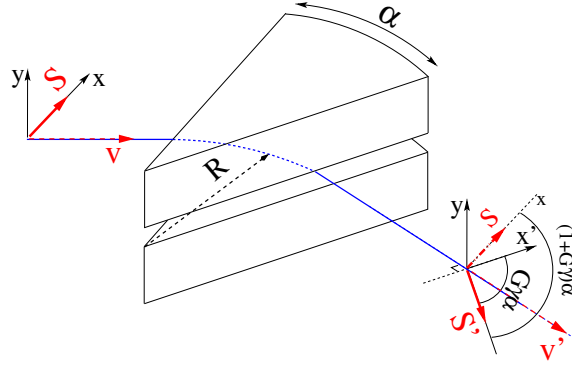
$$\frac{d\mathbf{S}}{dt} = \mathbf{S} \times \omega_{\text{sp}} \quad (3.32)$$

1144 If the particle moves in the median plane of a cyclotron then $\mathbf{B}_{\parallel} = 0$ and the
 1145 precession axis is parallel to the magnetic field vector, \mathbf{B}_y , namely $\omega_{\text{sp}} = \frac{q}{m} (1 +$
 1146 $G\gamma)\mathbf{B}_y$. The precession angle writes

$$\theta_{\text{sp, Lab}} = \frac{1}{v} \int \omega_{\text{sp}} ds = (1 + G\gamma) \frac{\int B ds}{BR} = (1 + G\gamma)\alpha \quad (3.33)$$

with α the trajectory bend angle (Fig. 3.17). The precession angle in the moving

Fig. 3.17 Spin and velocity vector precession in a constant field, from \mathbf{S} to \mathbf{S}' and \mathbf{v} to \mathbf{v}' respectively. In the moving frame the spin precession along the arc $\mathcal{L} = R\alpha$ is $G\gamma\alpha$, in the laboratory frame the spin precesses by $(1 + G\gamma)\alpha$



1147

1148 frame (the latter rotates by an angle α across the magnet) is

$$\theta_{\text{sp}} = G\gamma\alpha \quad (3.34)$$

1149

1150

1151

from what it results that the number of precessions per turn is $G\gamma$. By analogy with the betatron tune (the number of sinusoidal oscillations per turn around the reference circle, Eq. 3.17) this defines the spin tune

$$\nu_{\text{sp}} = G\gamma \quad (3.35)$$

1152 3.2 Exercises

1153 Preliminaries

- 1154 • Keywords in zgoubi: by “keyword” it is meant, the name of the optical elements
 1155 (such as DIPOLE, ELCYLDEF, MULTIPOLE, TOSCA, WIENFILTER, etc.), or
 1156 I/O procedures (such as FAISCEAU, FAISTORE, IMAGE, etc.), or commands
 1157 (such as FIT, SYSTEM, etc.), as they appear in a simulation input data file.
 1158 Keywords are most of the time referred to without any additional explanation in
 1159 the exercise solutions: details and explanations regarding the use and functioning
 1160 of keywords are to be found in the users’ guide.
- 1161 • It is strongly recommended, when setting up the input data files to work out the
 1162 exercises, to have Zgoubi users’ guide at hand. PART B of the guide in particular,
 1163 details the formatting of the input data which follow any keyword, and their units
 1164 (a few keywords only, for instance FAISCEAU, MARKER, YMY, do not require
 1165 additional data). PART A is the “physics content” and details what keywords
 1166 are doing and how. The users’ guide INDEX is a convenient tool to navigate
 1167 keywords. A complete list may also be found in the “Glossary of Keywords”, at
 1168 the beginning of both PART A and PART B of the users’ guide, and an overview
 1169 of what they can be used at is given in “Optical elements versus keywords”.
- 1170 – A concise notation KEYWORDS[ARGUMENT1, ARGUMENT2, ...] is used
 1171 in the exercises and solutions: it follows the nomenclature of the Users’ Guide,
 1172 Part B. A couple of examples:
 1173 • OBJET[KOBJ=1] stands for keyword OBJET, and the value of KOBJ=1
 1174 retained here;
 1175 • OPTIONS[CONSTY=ON] stands for keyword OPTIONS, and the option
 1176 retained here, CONSTY, switched ON.
- 1177 – The keyword INCLUDE is used in many simulation input data files. The
 1178 goal is mostly to reduce the length of these files (which would otherwise
 1179 be prohibitively voluminous, for a book). Just as with the Latex, or Fortran
 1180 “include” command, a segment of an optical sequence subject to an INCLUDE
 1181 in some input data file, may always be replaced by that very sequence segment
 1182 in plain.
- 1183 • Coordinate Systems: two sets of coordinate notations are used in the exercises,
 1184 – on the one hand (and, in the Solutions Section mostly), zgoubi’s (Y,T,Z,P,X,D)
 1185 coordinates in the optical element reference frame (O;X,Y,Z), the very frame
 1186 in which the optical element field $\mathbf{E}(X, Y, Z)$ and/or $\mathbf{B}(X, Y, Z)$ is defined (the
 1187 origin for X depends on the optical element). Particle coordinates in this frame
 1188 can be
 1189 • either Cartesian, in which case X, Y, and Z denote the particle position in
 1190 that frame, T and P the horizontal and vertical trajectory angles,
 1191 • or cylindrical, in which case, given m the projection of particle position
 1192 M in the $Z=0$ plane, Y denotes the radial coordinate: $Y = |\mathbf{Om}|$, whereas

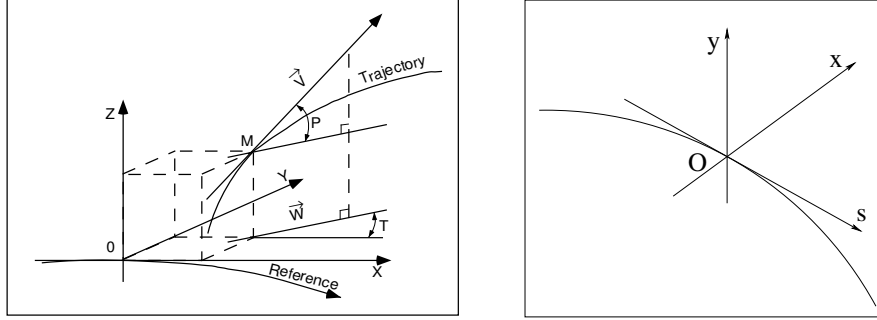


Fig. 3.18 Zgoubi Cartesian frame (O;X,Y,Z), and moving frame (O;s,x,y)

1193
1194
1195
1196

X denotes the polar angle $\mathbf{OX}-\mathbf{Om}$ (as a matter of fact, the nature of the variables named X and Y in the source code does change), T is the horizontal trajectory angle with respect to the normal to \mathbf{Om} , P is the vertical trajectory angle;

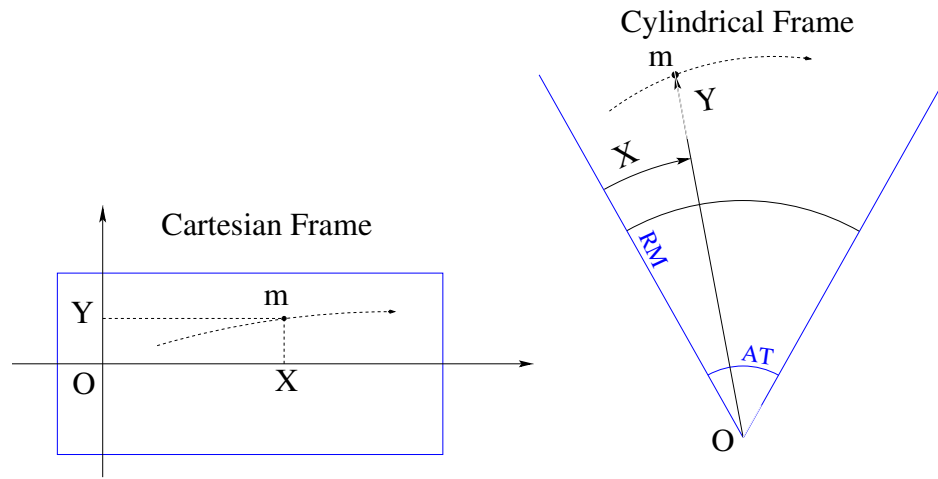


Fig. 3.19 Cartesian and cylindric reference frames in zgoubi. Let a particle location $M(X,Y,Z)$ project at $m(X,Y)$ (the dashed line figures the projected trajectory). In the case of an optical element (figured as a rectangular box) defined in Cartesian coordinates (case for instance of *MULTIPOL*, *BEND*, *TOSCA*[MOD ≤ 19]), X and Y in zgoubi.plt denote the coordinates taken along the reference frame axes. In the case of an optical element (figured as an angular sector AT with some reference radius RM) (case for instance of *DIPOLE*[S][-M], *TOSCA*[MOD ≥ 20]), X is the polar angle, counted positive clockwise, Y is the radius

Note: the sixth coordinate in zgoubi's set above is

$$D = \frac{\text{particle rigidity}}{BORO} = \frac{B\rho}{BORO}$$

with BORO a reference rigidity, the very first numerical datum to appear in any zgoubi sequence, as part of the definition of initial particle coordinates by OBJET or MCOBJET. BORO may sometimes be denoted $B\rho_{\text{ref}}$, depending upon the context. Note that D-1 identifies with the coordinate $\delta p/p$ below.

- on the other hand (and, in the exercise assignments mostly), the conventional $(x, x', y, y', \delta l, \delta p/p)$ coordinates in the moving frame (O;s,x,y) or close variants.

Comments are introduced wherever deemed necessary (hopefully, often enough) in an effort to lift potential ambiguities regarding coordinate notations.

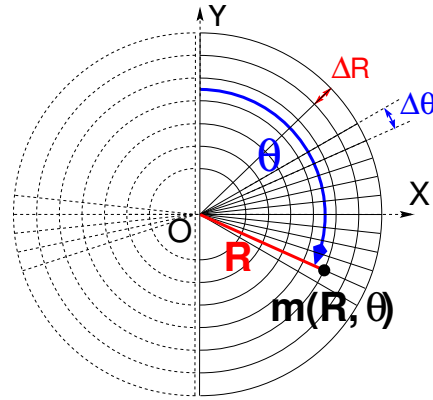
3.1 Modeling a Cyclotron Dipole: Field Map

In this exercise, a cyclotron dipole field is simulated using a field map. A field map is an easy way to simulate a magnet, this is a major interest of the method. It can account for fancy geometries and fields, including field index and non-linearities, field defects. Depending on field symmetries it may be 1-, 2-, or 3-dimensional. It can be generated using mathematical field models, or from magnet computation codes, or from magnetic measurements. In this exercise a model of a cyclotron field is devised using such field map method. The model is based on a calculated two-dimensional map of the mid-plane field, with 180 deg or 60 deg angular extent; TOSCA keyword is used to raytrace through these maps.

The first step in this exercise consists in fabricating that field map.

A 2-dimensional $m(R, \theta)$ polar meshing of the median plane is considered (Fig. 3.20). It is defined in a (O; X, Y) frame and covers a 180° sector (or 60 deg, in some of the exercises). The median plane field map provides the values of the field components $B_Z(R, \theta)$ normal to the $Z = 0$ plane, at the nodes of the mesh. Note that a single 360° field map could be used instead, however implementing two 180° sectors will allow further insertion of an accelerating gap, between the two 180° sectors. Computation of the field along (R, θ) particle trajectories in the (O;X,Y,Z) frame is performed from the field map data, using interpolation techniques [13].

Fig. 3.20 Principle of a field map in a polar coordinate system, covering a 180° sector (over the right hand side dee). The mesh nodes $m(R, \theta)$ are distant ΔR radially, $\Delta\theta$ azimuthally. The map is used twice, so covering the 360° cyclotron dipole as sketched here, while allowing further insertion of an accelerating gap between the two dees



(a) Construct a 180° two-dimensional map of a median plane field $B_Z(R, \theta)$, proper to simulate the field in a cyclotron as sketched in Fig. 3.1. Use a uniform mesh in a polar coordinate system (R, θ) as sketched in Fig. 3.20, covering from $R=1$ to 76 cm. Take a radial increment of the mesh $\Delta R = 0.5$ cm, azimuthal increment $\Delta\theta = 0.5$ cm/RM, RM some arbitrary reference radius (say, 50 cm, here), and constant axial field $B_Z = 0.5$ T. The appropriate 6-column formatting of the field map data for TOSCA to read them is the following:

$R \cos \theta, Z, R \sin \theta, B_Y, B_Z, B_X$

with θ varying first, R varying second in that list. Z is the vertical direction (normal to the map mesh), $Z \equiv 0$.

Produce a graph of $B_Z(R, \theta)$.

(b) Raytrace a few concentric circular mid-plane trajectories centered on the center of the dipole, ranging in $10 \leq R \leq 80$ cm. Produce a graph of these concentric trajectories in the $(O; X, Y)$ laboratory frame.

Initial coordinates can be defined using OBJET, particle coordinates along trajectories during the stepwise raytracing can be logged in zgoubi.plt by setting IL=2 under TOSCA. In order to find the Larmor radius corresponding to a particular momentum, the matching procedure FIT can be used. In order to repeat for a series of momenta, ERBELOTE[IOPT=1] can be used.

Explain why it is possible to push the raytracing beyond the 76 cm radius field map extent, without loss of accuracy.

(c) Compute the orbit radius R and the revolution period T_{rev} as a function of kinetic energy E_k , or rigidity BR . Produce a graph, including for comparison the theoretical dependence of T_{rev} . Explain what causes the slow increase of revolution period with energy.

(d) Check the effect of the density of the mesh (the choice of ΔR and $\Delta\theta$ values, i.e., the number of nodes $N_\theta \times N_R = (1 + \frac{180^\circ}{\Delta\theta}) \times (1 + \frac{80 \text{ cm}}{\Delta R})$), on the accuracy of the trajectory and time-of-flight computation.

(e) Consider a mesh with such $\Delta R, \Delta\theta$ density as to ensure reasonably good convergence of the numerical resolution of the differential equation of motion [13, Eq. 1.2.4].

Check the effect of the integration step size on the accuracy of the trajectory and time-of-flight computation, by considering a small $\Delta s = 1$ cm and a large $\Delta s = 20$ cm, at 200 keV and 5 MeV (assume proton).

(f) Consider a periodic orbit, thus its radius R should remain unchanged after stepwise integration of the motion over a turn. However, the size Δs of the numerical integration step has an effect on the final value of the radius:

for two different cases, 200 keV (a small orbit) and 5 MeV (a larger one), provide the dependence of the relative error $\delta R/R$ after one turn, on the integration step size Δs (consider a series of Δs values in a range $\Delta s : 0.1 \text{ mm} \rightarrow 20 \text{ cm}$). Plot the two $\frac{\delta R}{R}(\Delta s)$ curves (200 keV and 5 MeV), explain their upward concavity.

3.2 Modeling a Cyclotron Dipole: Analytical

This exercise is similar to exercise 3.1, the difference is that an analytical modeling of the field is used here, rather than a field map. The same polar coordinate system (R, θ, Z) is considered, with vertical axis Z normal to the (R, θ) plane (Fig. 3.21).

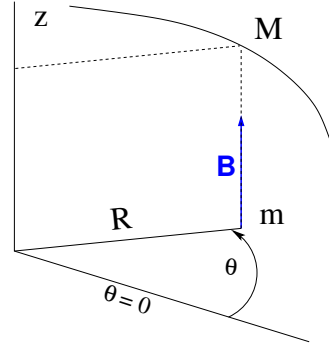


Fig. 3.21 Polar frame.
DIPOLE provides the value $B_Z(m)$ of the median plane field at m , projection of particle position $M(R, \theta, Z)$ in the median plane (R, θ)

The vector field $\mathbf{B}(R, \theta, Z)$ at any location $M(R, \theta, Z)$ of a particle along its trajectory is modeled using DIPOLE (a convenient choice among other possibilities found in zgoubi optical element library). DIPOLE provides the Z-parallel median plane field $\mathbf{B}(R, \theta, Z = 0) \equiv \mathbf{B}_Z(R, \theta, Z = 0)$, and $\mathbf{B}(R, \theta, Z)$ off the median plane is obtained by Taylor expansion (accounting for Maxwell's equations).

(a) Simulate a 180° sector dipole; DIPOLE requires a reference radius, R_M , for the sake of consistency with other exercises, it is suggested to take $R_M = 50$ cm. Take a constant axial field $B_Z = 0.5$ T.

Explain the various data (geometry, role of R_M , field and field indices, fringe fields, integration step size, etc.) that define the field simulation in DIPOLE - refer to the Users' Guide [13].

Produce a graph of $B_Z(R, \theta)$.

(b) Repeat question (b) of exercise 3.1.

(c) Repeat question (c) of exercise 3.1.

(d) As in question (e) of exercise 3.1, check the effect of the integration step size on the accuracy of the trajectory and time-of-flight computation.

Repeat question (f) of exercise 3.1.

(e) From the two series of results (exercise 3.1 and the present one), comment on various pros and cons of the two methods, field map versus analytical field model.

3.3 Geometrical Focusing

Because the field is constant over the all space ($\mathbf{B} \equiv \mathbf{B}_Z$ and $|\mathbf{B}_Z| = \text{constant}$, $\forall X, Y, Z$), there is no vertical focusing: any trajectory with a non-zero vertical angle would spiral away, vertically, with constant pitch angle.

(a) Using the foregoing field model, verify that this is what the numerical integration yields.

Produce a 3-D graph of the trajectory, superpose theory (use the parametric equations of motion) and numerical integration.

(b) Instead, horizontal motion features geometrical focusing, this is due to the trajectory curvature. Show the geometrical focusing graphically.

3.4 Relativistic Kinematic Relationships

In the subsequent exercises, relativistic kinematic quantities will be used, this exercises introduces some differential relations between them which will also be resorted to.

(a) Demonstrate the following relativistic relations (M =rest mass, E_k =kinetic energy, $E = E_k + M$, $c=1$; γ may vary in electrostatic elements or in the RF cavities of an accelerator):

$$\begin{aligned} \frac{dp}{p} &= \frac{1}{\beta^2} \frac{dE}{E}, & dp &= \frac{dE}{\beta} \\ \frac{dv}{v} &= \frac{d\beta}{\beta} = \frac{1}{\gamma^2} \frac{dp}{p} = \frac{1}{\beta^2 \gamma^2} \frac{dE}{E} = \frac{1}{\beta^2 \gamma^2} \frac{d\gamma}{\gamma} \\ \frac{d\gamma}{\gamma} &= \frac{dE}{E} = \frac{dE_k}{E_k + M} \\ \frac{dE}{E - M} &= \frac{dE_k}{E_k} = \frac{\gamma + 1}{\gamma} \frac{dp}{p} \end{aligned}$$

(b) Produce the evolution of these quantities numerically, compare these numerical results with theoretical expectations from (a).

(c) Using the random particle generator MCOBJET, produce a 2×10^4 bunch of protons with Gaussian dp/p , $\sigma_{dp/p} = 10^{-3}$. Plot some of the densities above and check the equalities in (a).

3.5 Resonant Acceleration (1)

Based on the earlier dipole sector, using indifferently a field map or an analytical model of the field, introduce an accelerating gap between the two dees with peak voltage 100 kV. Assume that particle motion does not depend on RF phase: the boost through the gap is the same at all passes, CAVITE[IOPT=3] can be used for that.

(a) Accelerate a proton with initial kinetic energy 20 keV, up to 5 MeV, take harmonic $h=1$. Produce a graph of the accelerated trajectory in a (O; X, Y) frame similar to that in Fig. 3.20.

(b) Plot the proton momentum p and total energy E as a function of its kinetic energy, both from this numerical experiment (raytracing data can be stored using FAISTORE) and from theory, everything on the same graph.

(c) Plot the normalized velocity $\beta = v/c$ as a function of kinetic energy, both numerical and theoretical, and in the latter case both classical and relativistic.

(d) Plot the relative change in velocity $\Delta\beta/\beta$ and the relative change in circumference $\Delta C/C$, as a function of kinetic energy. both numerical and theoretical. From their evolution, conclude that the time of flight increases with energy.

3.6 Resonant Acceleration (2)

Re-do the previous exercise, assuming a harmonic $h=3$ RF frequency.

3.7 Visit High Energies

Forget the fact that this not possible in a classical cyclotron (use CAVITE[IOPT=3]), and push proton energy to 3 GeV kinetic, re-do questions (a) to (d) of Ex. 3.5.

Note:

- pushing the energy in this manner is only possible if acceleration at the gap is independent of particle phase, hence the necessary choice of CAVITE[IOPT=3],

- 1338 - if a field map model is used, it is perhaps, or perhaps not, necessary to extend the
- 1339 radial extent of the mesh to encompass the spiraling trajectory up to 3 GeV - please
- 1340 clarify that point,
- 1341 - in the case the analytical model DIPOLE is used instead, surely no modification
- 1342 is needed, its data remain unchanged, figure that out.

1343 3.8 Spin Dance

- 1344 (a) From the analogy between the vector precession equations,
- 1345
$$\dot{\mathbf{v}} = \frac{q}{m} \mathbf{v} \times \mathbf{B},$$
 particle velocity vector, on the one hand
- 1346
$$\dot{\mathbf{S}} = \mathbf{S} \times \omega_{\text{sp}},$$
 particle spin vector, on the other hand (Eq. 20.28),
- 1347 and from the expression for the particle trajectory rotation angle $\alpha = \int B ds / BR$ as
- 1348 stems from the former, deduce the expression for the spin rotation angle in constant
- 1349 vertical B field - no calculations needed.

1350 In the following the cyclotron model of exercise 3.1 or 3.2 indifferently can be
1351 used.

- 1352 (b) Add spin transport, using SPNTRK. Produce a listing (zgoubi.res) of a simu-
1353 lation, including spin outcomes.

1354 Note: PARTICUL is necessary here, in order for the equation of motion to be
1355 solved [13, Sec. 2]. SPNPRT can be used to have local spin coordinates listed in
1356 zgoubi.res (at the manner FAISCEAU lists particle coordinates).

- 1357 (c) Consider proton case, initial spin longitudinal, compute the spin precession
1358 over one revolution, as a function of energy over a range 12 keV → 5 MeV. Give a
1359 graphical comparison with theory.

1360 FAISTORE can be used to store local particle data, which include spin coordi-
1361 nates, in a zgoubi.fai style output file. IL=2 can be used to obtain a print out of
1362 particle motion data to zgoubi.plt during stepwise integration.

- 1363 (d) Inject a proton with longitudinal initial spin S_z . Give a graphic of the longi-
1364 tudinal spin component motion as a function of azimuthal angle, over a few turns
1365 around the ring. Deduce the spin tune from this computation. Repeat for a couple of
1366 different energies.

1367 Place both FAISCEAU and SPNPRT commands right after the first dipole sector,
1368 and use them to check the spin rotation and its relationship to particle rotation, right
1369 after the first passage through that first sector.

- 1370 (e) Spin dance: the optical sequence here is assumed to be a complete turn (*i.e.*,
1371 six DIPOLES if a 60 deg DIPOLE model is used). Inject an initial spin at an angle
1372 from the horizontal plane (this is in order to have a non-zero vertical component),
1373 produce a 3-D animation of the spin dance around the ring, over a few turns.

- 1374 (f) Repeat questions (b-e) for two additional particles: deuteron (much slower
1375 spin precession), $^3\text{He}^{2+}$ (much faster spin precession).

1376 3.9 Synchronized Spin Torque

1377 A synchronized spin kick is superimposed on orbital motion. A input data file
1378 file accounting the simulation of a complete cyclotron is considered as in (e), for
1379 instance six 60 degree DIPOLES, or two 180 degree DIPOLES, etc.

1380 Insert a spin rotation of a few degrees around the longitudinal axis, at the end
 1381 of the optical sequence (*i.e.*, after one orbit around the cyclotron). SPINR can be
 1382 used for that, to avoid any orbital effect. Track 4 particles on their closed orbit, with
 1383 respective energies 0.2, 108.412, 118.878 and 160.746 MeV.

1384 Produce a graph of the motion of the vertical spin component S_y along the circular
 1385 orbit.

1386 Produce a graph of the spin vector motion on a sphere.

1387 Explain the results.

1388 3.10 Introducing a Radial Field Index

1389 (a) Reproduce Fig. 3.11.

1390 (b) Ray trace over a few turns with some $-1 < k < 0$ value, to show the sinusoidal
 1391 horizontal motion. Show the horizontal motion instability when $k < -1$.

1392 (c) Add vertical motion and show the vertical sinusoidal oscillation with $k < 0$,
 1393 show the vertical instability if $k > 0$.

1394 3.11 Weak Focusing

1395 (a) Consider a 60° sector as in earlier exercises (building a field map as in
 1396 exercise 3.1, or using DIPOLE as in exercise 3.2), construct the sector accounting
 1397 for a non-zero radial index k in order to introduce vertical focusing, say $k = -0.03$,
 1398 assume a reference radius R_0 for a reference energy of 200 keV (R_0 and B_0 are
 1399 required in order to define the index k , Eq. 3.12). Raytrace that 200 keV reference
 1400 orbit, plot it in the lab frame: make sure it comes out as expected, namely, constant
 1401 radius, final and initial angles equal (normally null given the working hypotheses, as
 1402 established in previous exercises).

1403 (b) Find and plot the radius dependence of orbit rigidity, $BR(R)$, from raytracing
 1404 over a BR range covering 20 keV to 5 MeV.

1405 (c) Produce a graph of the paraxial axial motion of a 1 MeV proton, over a
 1406 few turns (use $IL=2$ under TOSCA to have stepwise integration data logged in
 1407 `zgoubi.plt`). Check the effect of the focusing strength by comparing the trajectories
 1408 for a few different index values, including close to -1 and close to 0.

1409 (d) Produce a graph of the magnetic field experienced by the particle along these
 1410 trajectories.

1411 3.12 Loss of Isochronism

1412 Compare on a common graphic the revolution period $T_{\text{rev}}(R)$ for a field index
 1413 value $k \approx -0.95, -0.5, -0.03, 0^-$. The scan method of exercise 3.11, based on
 1414 REBELOTE, can be referred to.

1415 3.13 Particle Trajectories

1416 In this exercise individual particle trajectories are computed. DIPOLE or TOSCA
 1417 can be used, indifferently. No acceleration in this exercise, particles cycle around the
 1418 cyclotron at constant energy.

1419 (a) Produce a graph of the horizontal and vertical trajectory components $x(s)$ and
 1420 $y(s)$ of a particle with rigidity close to $BR(R_0)$ (R_0 is the reference radius in the
 1421 definition of the index k), over a few turns around the cyclotron. From the number of

turns, give an estimate of the wave numbers. Check the agreement with the expected $\nu_R(k)$, $\nu_y(k)$ values from Eq. 3.17.

Consider particle energies of 1 MeV and 5 MeV, far from the reference kinetic energy $E(R_0)$; the wave numbers change with energy: could that be expected? Find their theoretical values, compare with numerical outcomes.

(b) In the former case, 200 keV energy, plot as a function of s the difference between $x(s)$ from raytracing and its values from Eq. 3.15. Same for $y(s)$ compared to Eq. 3.16. Is there agreement? (use the option $IL=2$ to store particle coordinates in `zgoubi.plt`, step-by-step).

3.14 Energy Dependence of Wave Numbers

Perform a scan of the wave numbers over 200 keV–5 MeV energy interval, computed using MATRIX, and using REBELOTE to repeat MATRIX computation for a series of energy values.

3.15 Phase Space Motion, Fourier Analysis

This exercise introduces to phase space and phase space motion, and to spectral analysis of particle motion.

Raytrace a particle with small amplitude radial and axial oscillations with respect to the reference circular closed orbit (paraxial motion), at constant energy.

(a) At some fixed azimuth s around the cyclotron, observe the radial excursion $(x(n), x'(n))$ of the particle as it cycles around for many turns (n is the turn number) (use FAISTORE to store particle coordinates in `zgoubi.fai`, turn by turn). Produce a graph of $(x(n), x'(n))$ in the transverse phase-space (x, x') .

Repeat for (y, y') .

(b) From the trajectory equation (Eq. 3.15, radial motion, or Eq. 3.16, axial motion), show that particle motion in phase space is on an ellipse. Calculate the ellipse parameters. Verify graphically that it superposes on the particle motion from multiturn raytracing.

(c) Compute the radial and axial wave numbers by Fourier analysis of respectively the $x(n)$ and the $y(n)$ motion. Check the agreement with the expected $\nu_R(k)$, $\nu_y(k)$ values from theory.

(d) Constant energy motion spectrum:

(i) there is an indetermination on the value of the wave number, from the Fourier analysis, explain

(ii) give a theoretical calculation of the accuracy on the position of the peak from the DFT technique. Check this against the numerical computation by varying the spectrum sampling in the DFT series

(iii) explain the origin of the $\sin u/u$ shape of the spectrum. Calculate the spacing between the zeroes, from theory, compare with the zeroes of the numerical DFT.

3.16 RF Phase at the Accelerating Gap

(a) Consider the cyclotron model of exercise 3.11: two dees, double accelerating gap, field index $k = -0.03$ defined at $R_0 = 50$ cm, field $B_0 = 5$ kG on that radius.

Raytrace a proton trajectory from 1 to 5 MeV: get the turn-by-turn phase-shift at the gaps, compare with (Eq. 3.26)

$$\text{half-turn } \Delta\phi = \pi \left(\frac{\omega_{\text{rf}}}{\omega_{\text{rev}}(R)} - 1 \right) = \pi \left(\frac{m\omega_{\text{rf}}}{qB(R)} - 1 \right)$$

1463 Produce a similar diagram $\Delta W(\phi)$ to Fig. 3.14-right.

1464 Accelerate over more turns, observe the particle decelerate.

1465 (b) Repeat (a) for the index definition of exercise 3.11: $k=-0.03$, defined on the
1466 200 keV injection radius $R_0 = 12.924888$ cm, with $B_0 = 5$ kG.

1467 3.17 The Cyclotron Equation

1468 Cyclotron model settings of exercise 3.5 are first considered in questions (a) to (c):
1469 two dees, double accelerating gap, uniform field $B = 0.5$ T (a field map or analytical
1470 field modeling can be used, indifferently). In question (d) a field index is introduced.

1471 (a) Set up an input data file for the simulation of a proton acceleration from
1472 0.2 to 20 MeV. In particular, assume that $\cos(\phi)$ reaches its maximum value at
1473 $W_m = 10$ MeV; find the RF voltage frequency from $d(\cos \phi)/dW = 0$ at W_m .

(b) Give a graph of the energy-phase relationship (Eq. 3.27)

$$\cos \phi = \cos \phi_0 + \pi \left[1 - \frac{\omega_{\text{rf}}}{\omega_{\text{rev}}} \frac{E + E_0}{2M} \right] \frac{E - E_0}{q\hat{V}}$$

1474 for $\phi_0 = \frac{3\pi}{4}, \frac{\pi}{2}, \frac{\pi}{4}$, from both simulation and theory.

1475 (c) Re-do the exercise using an RF frequency third harmonic of the revolution
1476 frequency, in the same double-dee configuration.

1477 (d) Repeat (a) and (b) for the index definition of exercise 3.11: $k=-0.03$, defined
1478 on the 200 keV injection radius $R_0 = 12.924888$ cm, with $B_0 = 5$ kG.

1479 3.18 Cyclotron Extraction

1480 (a) Acceleration of a proton in a uniform field $B=0.5$ T is first considered, this is
1481 the case of exercise 3.5.

1482 Compute the distance ΔR between turns, as a function of turn number and of
1483 energy, over the range $E : 0.02 \rightarrow 5$ MeV. Compare graphically with theoretical
1484 expectation.

1485 (b) Assume a beam with Gaussian momentum distribution and *rms* momentum
1486 spread $\delta p/p = 10^{-3}$. An extraction septum is placed half-way between two successive
1487 turns, plot the percentage of beam loss at extraction, as a function of extraction turn
1488 number - COLLIMA can be used for that simulation and for particle counts, it also
1489 allows for possible septum thickness.

1490 (c) Repeat (a) and (b) considering a field with index - conditions of exercise 3.10
1491 for instance, $B_0 = 0.5$ T and $k = -0.03$ at $R_0 = R(0.2 \text{ MeV}) = 12.924888$ cm.

1492 (d) Investigate the effect of injection conditions (x_0, x'_0) on the modulation of the
1493 distance between turns.

1494 Show that, with slow acceleration, the oscillation is minimized for an initial
1495 $|x'_0| = \left| \frac{x_0 v_R}{R} \right|$ [8, p. 133].

1496 3.19 Acceleration and Extraction of a 6-D Polarized Bunch

1497 The cyclotron simulation hypotheses of exercise 3.17-a are considered.

1498 Add a short “high energy” line, say 1 meter, for beam extraction downstream of
 1499 the cyclotron (which means following REBELOTE in the optical sequence), ending
 1500 up with a “Beam_Dump” MARKER.

1501 (a) Create a 1,000 particle bunch with the following initial parameters:

1502 - random Gaussian transverse phase space densities, centered on the closed orbit,
 1503 truncated at 3 sigma, normalized *rms* emittances $\varepsilon_Y = \varepsilon_Z = 1 \pi \mu\text{m}$, both emittances
 1504 matched to the 0.2 MeV orbit optics,

1505 - uniform bunch momentum density $0.2 \times (1 - 10^{-3}) \leq p \leq 0.2 \times (1 + 10^{-3}) \text{ MeV}$,
 1506 matched to the dispersion, namely (Eq. 3.21), $\Delta x = D \frac{\Delta p}{p}$,

1507 - random uniform longitudinal distribution $-0.5 \leq s \leq 0.5 \text{ mm}$,

1508 Note: there is two possibilities to create this object, namely, using either
 1509 (i) MCOBJET, or (ii) OBJET[KOBJ=3] which reads an external file containing
 1510 particle coordinates.

1511 Add spin tracking request (SPNTRK), all initial spins normal to the bend plane.

1512 Produce a graph of the three initial 2-D phase spaces: (Y,T), (Z,P), ($\delta l, \delta p/p$),
 1513 check the matching to the 200 keV optics.

1514 Plot the Y, Z, dp/p , δl and S_Z histograms. Check the distribution parameters.

1515 (b) Accelerate this polarized bunch to 20 MeV, using the following RF conditions:

1516 - 200 kV peak voltage,

1517 - RF harmonic 1,

1518 - initial RF phase $\phi_0 = \pi/4$.

1519 Produce a graph of the three phase spaces as observed downstream of the ex-
 1520 traction line. Plot the Y, Z, dp/p , δl and S_Z histograms. Compare the distribution
 1521 parameters with the initial values.

1522 What causes the spins to spread away from vertical?

References

- 1524 1. Jones, L., Mills, F., Sessler, A., et al.: Innovation Was Not Enough. World Scientific (2010)
- 1525 2. Lawrence, E.O., Livingston, M.S., Phys. Rev. 37, 1707 (1931), 1707; Phys. Rev. 38, 136,
- 1526 (1931); Phys. Rev. 40, 19 (1932)
- 1527 3. Ernest O. Lawrence and M. Stanley Livingston, The Production of High Speed Light Ions
- 1528 Without the Use of High Voltages, Phys. Rev. 40, 19-35 (1932)
- 1529 4. Livingston, M.S., McMillan, Edwin M.: History of the cyclotron. Physics Today, 12(10)
- 1530 (1959).
- 1531 <https://escholarship.org/uc/item/29c6p35w>
- 1532 5. Bethe, H. E., Rose, M. E.: Maximum energy obtainable from cyclotron. Phys. Rev. 52 (1937)
- 1533 1254
- 1534 6. Cole, F.T.: O Camelot ! A memoir of the MURA years (April 1, 1994).
- 1535 <https://accelconf.web.cern.ch/c01/cyc2001/extra/Cole.pdf>
- 1536 7. 4.a L.H.Thomas, *The Paths of Ions in the Cyclotron*, Phys. Rev. 54, 580, (1938)
- 1537 4.b M.K. Craddock, *AG focusing in the Thomas cyclotron of 1938* , Proceedings of PAC09,
- 1538 Vancouver, BC, Canada, FR5REP1
- 1539 8. Stambach, T.: Introduction to Cyclotrons. CERN accelerator school, cyclotrons, linacs and
- 1540 their applications. IBM International Education Centre, La Hulpe, Belgium, 28 April-5 May
- 1541 1994.
- 1542 9. Baron, E., et al.: The GANIL Injector. Proceedings of the 7th International Conference on
- 1543 Cyclotrons and their Applications, ZÃijrich, Switzerland (1975).
- 1544 <http://accelconf.web.cern.ch/c75/papers/b-05.pdf>
- 1545 10. Li, C.Y., et al.: A Permanent Magnet System for a Cyclotron used as a mass spectrometer.
- 1546 11. Lawrence, E.O., Edlefsen, N.E.: On the production of high speed protons. Science, 72, 376-377
- 1547 (1930)
- 1548 12. Le Duff, J.: Longitudinal beam dynamics in circular accelerators. CERN Accelerator School,
- 1549 Jyvaskyla, Finland, 7-18 September 1992
- 1550 13. Méot, F.: Zgoubi Users' Guide.
- 1551 <https://www.osti.gov/biblio/1062013-zgoubi-users-guide> Sourceforge latest version:
- 1552 <https://sourceforge.net/p/zgoubi/code/HEAD/tree/trunk/guide/Zgoubi.pdf>